Scientific Research Publishing

Sulfide Stress Cracking Assessment of Carbon Steel Welding with High Content of H₂S and CO₂ at High Temperature: A Case Study

Apolinar Albiter [ORCID]

Instituto Mexicano del Petróleo, Ciudad de México, México
Email: aalbiter@imp.mx

Abstract

In the oil and gas industry, it has been established that for pipelines fabricated with carbon steels, their limitation is related to H_2S and CO_2 environments, which is 7 to 10 psia of partial pressure of CO_2. Therefore, in carbon steel cracking is shown, after 7 or 10 psia of partial pressure of CO_2. The experimental work was performed under static conditions in autoclaves within a pH of 3 to 3.8; partial pressures of 16 - 96 psi for H_2S and 15 - 53 psi for CO_2, in the temperature range of 25°C - 150°C. It was observed that the average yielding stress used in Sulfide Stress Cracking (SSC) tests decreases with temperature increment. Hydrogen Induced Cracking (HIC) evaluations showed that X52 steel, under conditions, was not susceptible to HIC. Results of SSC did not show indications of cracking after exposure to sour solutions, except for the specimen exposed to high H_2S and CO_2 content (96 psi of H_2S and 53 psi of CO_2 of the partial pressure) and high temperature (150°C). Microcracks located between the upper and lower weld beads were also observed. However, the highest average corrosion rate was 0.27 mm/year (10.6 mpy), which occurred in samples exposed to 96 psi of H_2S and 53 psi of CO_2 at 150°C. Likewise, the highest localized corrosion (severe pitting attack) was obtained at the same environment with a corrosion rate of 4.2 mm/year (167 mpy). The oil and gas industry could use carbon steels pipelines in partial pressure higher than 10 psia.

Keywords

Sulfide Stress Cracking (SSC), Hydrogen Induced Cracking (HIC), Pitting, Welding, X52 Steel

1. Introduction

The oil and gas industry can provoke a wide variety of corrosive environments.

Mexican crude oil and gas commonly contain entrained water, carbon dioxide (CO_2), hydrogen sulfide (H_2S), high H_2S and CO_2 contents and heavy oil. Therefore, the transportation of these corrosive fluids always results in the induce of failures in the production systems; this shows the need to perform qualification tests on candidate pipelines steels considered for the development of the Mexican field, due to the high concentrations of H_2S and CO_2 expected in the exploitation of mature fields.

Sulfide stress cracking (SSC) is a major concern for most oil and gas pipeline operators for many years; however research work still is done to develop strategies for a better management of this problem [1]-[7]. It is well known that long-term operation of pipelines causes degradation of its mechanical properties, such as embrittlement caused by SCC [2]. The SCC occurs due to the combination of three factors; a susceptible material, localized tensile stress above a threshold and exposure to corrosive environment. However, sometimes due to environmental conditions, only corrosion occurs with no cracking [8]; nonetheless in many times the cracks evolve from corrosion pitting [9].

Due to the presence of H_2S, many metals are susceptible to: generalized, localized, pitting, and linear corrosion [10]. Therefore, most research focuses on the rules and mechanisms of hydrogen damage, such as sulfide stress corrosion cracking (SSC) and hydrogen-induced cracking (HIC), as well as the effect of environmental factors (temperature, partial pressure of H_2S, solution, and pH) on the corrosion process [11].

Among the technological challenges being faced to put such corrosive hydrocarbon's fields into production, material selection for corrosive environments is one of the most challenging. Materials selection requires knowledge of chemical and physical characteristics of the corrosive environment, along with the operation conditions at which the material will be exposed, in order to ensure good performance of the installations during his expected operational life. The high pressure along with the CO_2 content variable makes it impossible to use carbon steel in well, risers and topsides piping's; therefore it is required to use Corrosion Resistant Alloys (CRAs) [12].

The understanding of corrosion mechanisms in the combined presence of H_2S and CO_2 acidic gases has been discussed as a systematic approach for materials design strategy for hydrocarbon production systems. But, such approach does not deal with the important environmental cracking characteristics associated with sour service; nonetheless it concentrates purely on metal loss degradation process [13]. The combination of H_2S and CO_2 modifies the corrosion characteristics significantly as compared to damage caused in the sole presence of CO_2 or H_2S.

Both CO_2 and H_2S are acid gases which when produced with the hydrocarbon phase can render the associated water (condensed of formation) producing a very corrosive environment leading to severe degradation. The selection of materials to resist such corrosive environment relies mainly on the type of corrosion anticipated (e.g. general or localized), the confidence in predicting the rate and type of corrosion, risk of failure and life cycle cost. While the primary con-

cern in selection of materials in H_2S containing systems is the sulfide stress cracking (SSC); however the issue of corrosion should not be underestimated.

The purpose of this study was to evaluate the susceptibility of API X52 steel to environmental cracking, calculate general corrosion rates and analysis of localized corrosion in different sour environments. Therefore, X52 steel pipe samples were exposed to brine solutions with acid pH (3 to 3.8) and high concentrations of H_2S (16 to 96 psi of partial pressure) and CO_2 (15 to 53 psi of partial pressure) and high temperature (25°C to 150°C).

2. Experimental Procedure

2.1. Steel Analyzed

The steel used for the assessment of SSC behavior, corrosion and hydrogen induced cracking was an API X52 pipeline steel. The chemical composition of the steel is shown in Table 1. For experimental tests, a section of X52 steel with longitudinal and circumferential welding was used. Steel samples were obtained from a pipeline with an external diameter of 508 mm (20 in) and a wall thickness of 19.05 mm (0.750 in). Therefore, microstructural characterization through optical microscopy of the longitudinal and circumferential welding, along with the base metal and weld was carried out.

2.2. Hardness Tests

Vickers hardness measurements were carried out on sections of the welding joints of API X52 steel to verify compliance with the ANSI/NACE MR 0175/ISO 15156 [14] restriction, referring to the maximum hardness that should not be exceed 22 Rockwell C scale (248 HV) in order to avoid SSC problems.

2.3. Tensile Tests

Tensile tests were performed according to ASTM E21 [15] for each test temperature in order to characterize the steel before performing the SSC tests. The tests temperatures were 25°C, 50°C, 65°C, 80°C, and 150°C. The measured yield strength was used to stress the Four Point Bend Beam specimens. The small-size samples, similar to standard specimens, were used for tensile tests according to ASTM E8 [16], the cylindrical specimen with threaded ends was machined with a diameter of 6.35 mm (0.250 in), fillet radius of 7.74 mm (0.187 in), a reduced length section of 28.57 mm (1.125 in) and the gage length was 25.4 mm (1 in).

2.4. Hydrogen Induced Cracking Tests (HIC)

HIC tests were conducted on the samples obtained from API X52 steel with dimensions according to ANSI/NACE TM 0284 [17]. The HIC specimens were machined with 20 mm of width, 100 mm in length and full wall thickness of the pipe. Duplicate specimens were obtained from the circumferential weld, longitudinal weld and parent material; from the parent material one specimen was machined at 90 and 180 degrees from weld as shown in Figure 1.

Table 1. Chemical composition of API X52 steel (wt%).

C	Si	Mn	P	S	Ni	Cr	Cu	Mo	V	Nb	Ti	N	B	Al
0.06	0.190	0.92	0.012	0.002	0.120	0.120	0.210	0.020	0.045	0.045	0.015	0.004	0.0002	0.033
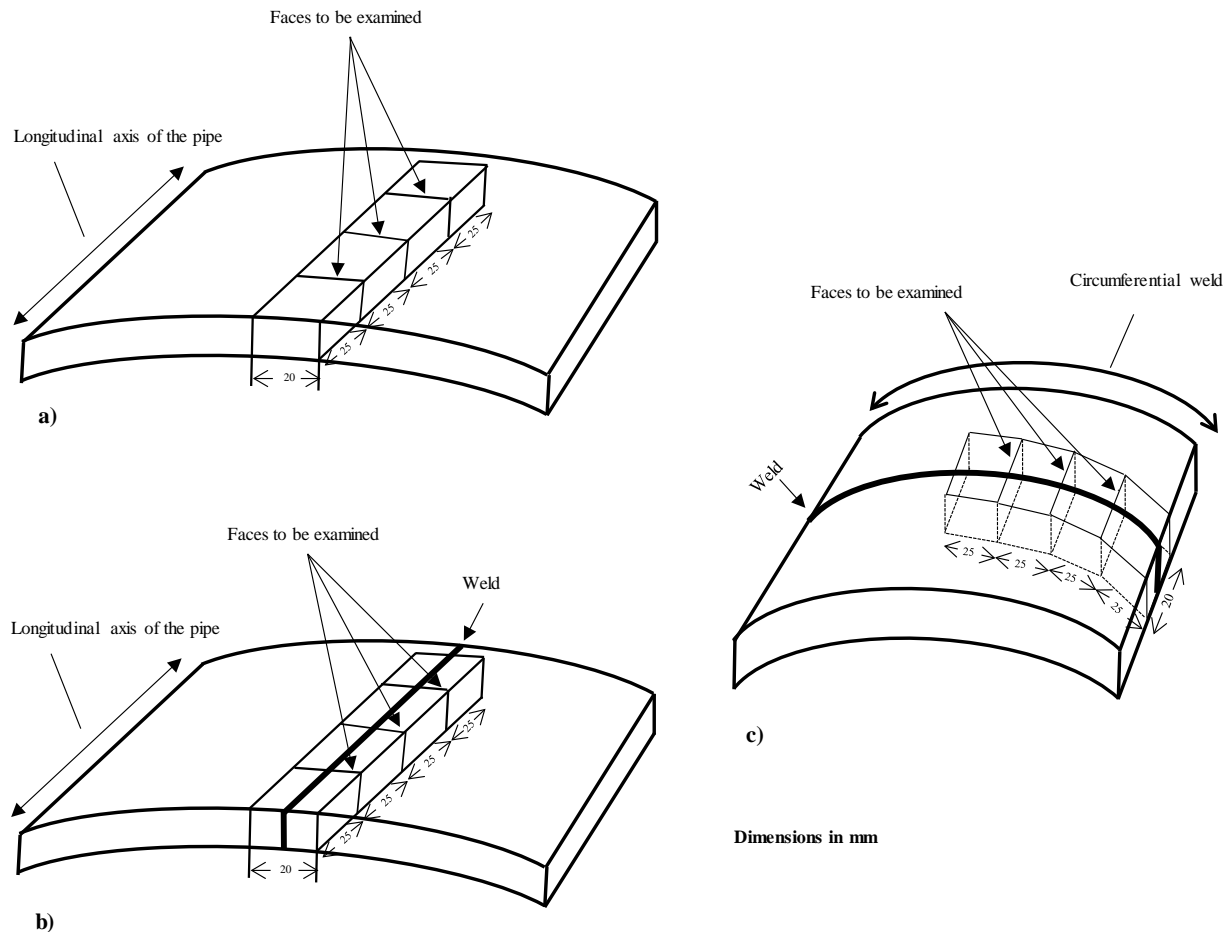
Figure 1. Specimen position and orientation for HIC testing: (a) parent metal, (b) longitudinal weld, and (c) circumferential weld.

The specimens were milled using coolant to avoid excessive overheating. After milling, the specimens were wet grinded with 320-grade SiC grinding paper. A minimum amount of material, up to 1 mm maximum, shall be removed from the inner and outer pipe surfaces in order to remove oxidation and provide prismatic specimens. After the specimens were ultrasonically cleaned (by immersion) with a detergent solvent, it was flushed with methanol or acetone and warm air-dried.

The formulations for the test solutions used to create the sour environments are described in Table 2, with a modified brine solution with pH of 3.0. HIC tests were performed using solution A. The temperature of the test solution was 25˚C a schematic sketch of the test assembly is shown in Figure 2.

The specimens were submerged in the brine solution and saturated with hydrogen sulfide at room temperature and it was maintained at a positive pressure during the 96-hour test duration and following test procedure:
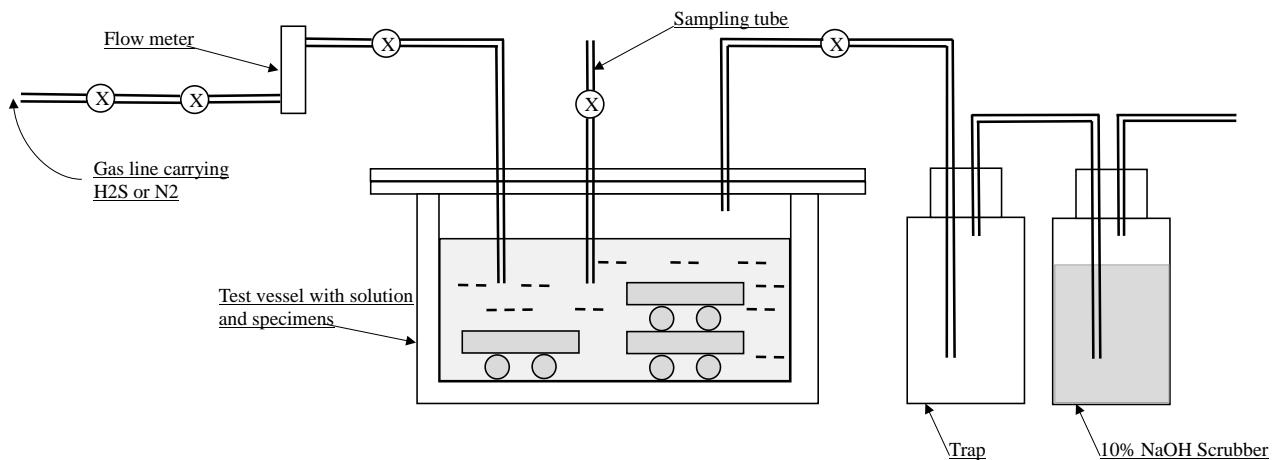
Figure 2. Schematic of the experimental arrangement for HIC testing.

Table 2. Chemical composition of brine solutions.

Reactive		Solution A	Solution B[a]
		Concentration (ppm)	Concentration (ppm)
Cations	Sodium (Na)	42,462	49,378
	Magnesium (Mg)	729	2860
	Calcium (Ca)	14,400	16,167
	Iron (Fe)	6	0.1
Anions	Chloride (Cl)	92,336	112,900
	Sulphate (SO$_4$)	900	175
	Bicarbonate (HCO$_3$)	386	100

[a]Solution used for one test a high pressure and high temperature (HP/HT).

- The test brine solution was prepared and transferred to the glass-purging vessel (Figure 2), ensuring that the volume of the test solution was sufficient to cover all of the test specimens.
- The specimen was separated from the vessel floor and other test specimens by suitable non-metallic rods with a minimum diameter of 6 mm.
- Purge test vessel with Nitrogen after purge the test solution, within the sealed purging vessel, with Nitrogen for at least 1 hour at minimum rate or 100 ml/min/liter of test solution.
- Transfer the test solution from de purging vessel to the vessel via the airtight filing tube, purge test solution, within the test vessel, with Nitrogen for at least 1 hour at minimum rate or 100 ml/min/liter of test solution.
- Following the Nitrogen purge, the solution shall be saturate with 99.5% H$_2$S gas, at a minimum rate of 200 ml/min/liter of the test solution for a minimum time of 60 minutes in the test vessel.
- Extract a sample from the solution, via the sampling tube and measure the pH and the H$_2$S concentration. If the H$_2$S concentration is >2300 ppm and the pH is within the specified range, the H$_2$S gas will then be passed through

the test solution for a period of 96 hours at a minimum flow rate in order to maintain a positive pressure. If not, continue saturation till H_2S concentration is >2300 ppm.

- After the 96-hour exposure period, draw a sample of the solution and measure pH and H_2S concentration. Stop the H_2S flow and purge the solution with Nitrogen at 200 ml/liter per hour flow rate for one-hour minimum to flush out all the H_2S from the test solution.

After exposure for 96 hours, the specimens were removed, cleaned and sectioned for metallographic examination.

The cleaned specimens were visually inspected and sectioned as shown in **Figure 1**. Each section was grounded, polished and etched in order to being observed in the optical microscope.

Based on the crack measurement results, the crack sensitivity ratio (CSR), the crack length ratio (CLR), and the crack thickness ratio (CTR) were calculated for each section and the average for each test specimen according to the following equations:

$$\text{CSR} = \frac{\sum(a \times b)}{(W \times T)} \times 100 \tag{1}$$

$$\text{CLR} = \frac{\sum(a)}{W} \times 100 \tag{2}$$

$$\text{CTR} = \frac{\sum(b)}{T} \times 100 \tag{3}$$

where a is crack length, b is the crack thickness, W is the section width and T is the test specimen thickness.

All identifiable cracks, visible at magnification up to 100× (10× objective lens) in the calculation, was included. Sometimes it was necessary to examine at higher magnifications to distinguish between small cracks, inclusions, pits or other discontinuities.

2.5. Sulfide Stress Cracking (SSC) at Low Pressure (LP) and High Temperature and High Pressure (HT/HP)

SSC tests were performed according to NACE TM 0177 [18], method B and EFC Publication: 16 "Guidelines on Material Requirements for Carbon and Low Alloy Steels for H_2S—Containing Environments in Oil and Gas Production" [19].

Four Point Bent-Beam (FPBB) specimens, fabricated from API X52 pipeline steel were machined and tested. The specimens were machined close to the ID with the weld located on the center of the specimen as is shown in **Figure 3**. Specimen's dimensions were approximately 119.4 × 19.05 × 4.83 mm (4.7 × 0.75 × 0.19 in). Prior to testing, the specimens were measured, cleaned and degreased in accordance with ASTM F21 [20].

The FPBB specimens were stressed up to 80% of the Actual Yield Strength (AYS) for each test temperature. Tensile testing was performed on each material to determine the AYS at different temperatures. The stresses were measured us-

ing two strain gauges attached adjacent to the weld as is shown in **Figure 3**. The stress was applied on the root weld surface (ID in tension). The stresses were recorded by the means of strain gauges on each side of the weld.

The stressed FPBB specimens were exposed in triplicate to each sour environment to simulate the field conditions. The exposure time was 720 hours and the environments consisted of two solutions (A and B) saturated. The summary of the FPBB tests conditions for the SSC testing and corrosion tests are presented in **Table 3**.

Eight liters of solution were prepared for testing and deaerated by purging with nitrogen. The stressed specimens and the mass-loss coupons were placed into the vessel and seal dry. After the solution was transferred into the vessel, then it was purged with nitrogen for eight hours. **Figure 4** shows the specimens and set-up before the exposure.

Table 3. Testing conditions for corrosion tests and SSC assessment.

Test No.	SSC		Corrosion Tests	Partial pressure (psi)		CO_2/H_2S ratio	Temperature (°C)		pH solution	
	LP	HP/HT		H_2S	CO_2		T1	T2	A	B
1	X	-	X	8	-	-	25	-	3	-
2	X	-	X	16	-	-	25	-	3	-
3	-	X	X	16	15	0.937	50	-	3.8	-
4	-	X	X	16	15	0.937	-	80	3.8	-
5	-	X	X	45	35	0.777	50	-	3.5	-
6	-	X	X	45	35	0.777	-	80	3.5	-
7	-	X	X	24.4	18.8	0.770	65	-	3.5	-
8	-	X	X	83	45	0.542	-	150	3.5	-
9	-	X	X	96	53	0.552	-	150	-	3.5
10	-	X	X	13.5	10	0.740	50	-	3.8	-
11	-	X	X	13.5	10	0.740	-	80	3.8	-

OD - Outside Diameter

ID - Inside Diameter
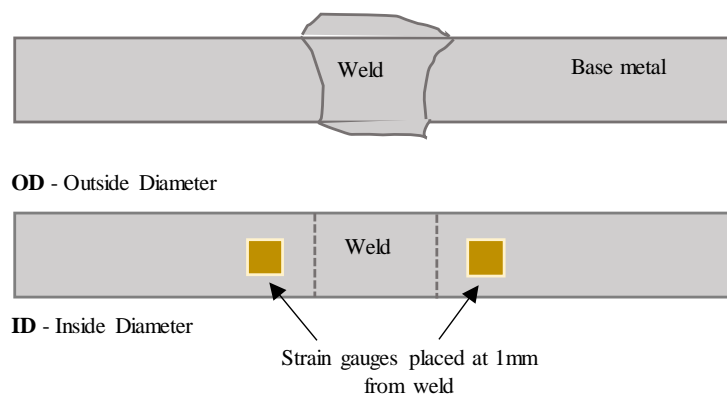
Strain gauges placed at 1mm from weld

Figure 3. Location of strain gauges used to measure the apply stress in the FPBB tests.
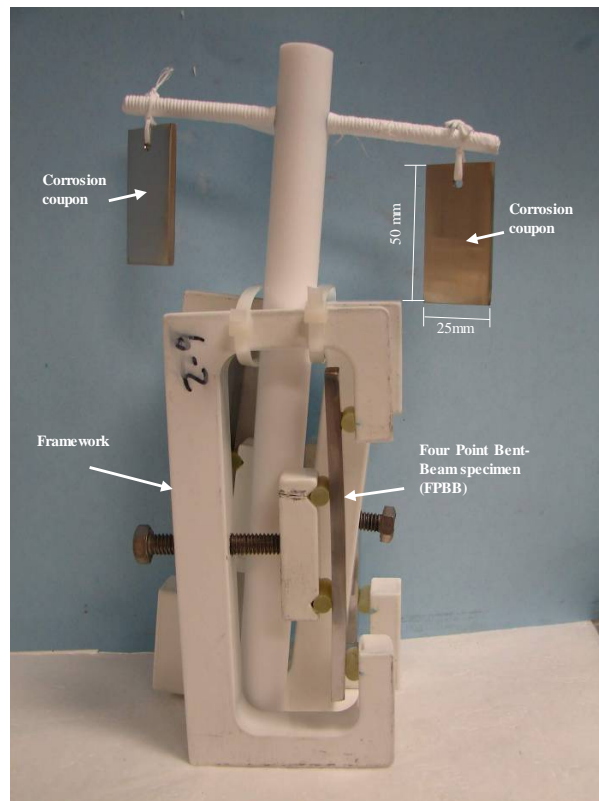
Figure 4. FPBB and mass-loss coupons set-up before testing.

For the exposure with total pressures below 16 psi, the solution was saturated with the respective brine solution A. The brine solution was saturated at room temperature and then the temperature was increased. Once the thermal equilibrium was achieved, the conditions were maintained during all time testing.

Upon completion of the exposures, the pH of the solutions was measured at room temperature. The FPBB specimens were removed, cleaned, and visually examined at a magnification of 10× to determine the presence of cracking. The cracking assessment was performed according to the NACE TM 0177 [18] and EFC Publication 16 [19]. Metallographic analysis was performed on all FPBB specimens after testing.

2.6. Corrosion Testing

Twenty-two coupons were machined from the API X52 steel; the dimensions are $50 \times 25 \times 3$ mm ($2.0 \times 1.0 \times 0.125$ inches) as is shown in **Figure 4**. Corrosion testing was performed on API X52 steel coupons according to ASTM G 111 [21]. The coupons were tested in duplicate in each sour environment. The conditions for corrosion testing were summarized in **Table 3**.

FPBB specimens and mass-loss coupons were exposed in the same vessel for each test environment during 720 hours. Eleven environments were created in the laboratory to simulate the different field conditions; the environments consisted of two solutions (A and B) saturated with nine gas mixtures at five test

temperatures. All the test was performed under static conditions in autoclaves with temperature and pressure control, in glass containers for low pressure tests.

After the 720 hours' exposure time, the mass-loss coupons were removed and photographed to document the surface appearance. Then, the coupons were cleaned to remove corrosion products according to specifications of ASTM G1 [22], rinsed in toluene/acetone, dried and re-weighed. General corrosion rates of each coupon were calculated according to the following equation.

$$CR(mpy) = \frac{534 * W}{\rho * A * T} \tag{4}$$

where W is the weight loss (mg), ρ is the density (g/cm³), A is the area (in²) and T is the time (hours).

The coupons were visually examined at a magnification of 50× to find evidences of localized corrosion. Any pitting was further characterized according to the specification of ASTM G46 [23].

The pitting depth was determined using optical measurements with an inverted metallurgical microscope and verified with a micrometer. The technique consists on initially focusing on the undamaged surface of the coupon and then re-focusing on the bottom of the pit. The difference in optical stage height is then converted to units of length. This length is reported in mils (0.001 inch) and corresponds to the pit depth. Once the maximum depth is established, the penetration rate is calculated using the ratio of 365 days/time exposed. The penetration rate is given in mils per year (mpy) units.

3. Results and Discussion

3.1. Microstructural Characterization

Figure 5(a) and Figure 5(b) show an optical microscopy image of the longitudinal and circumferential welds. The longitudinal weld was performed using the submerged metal arc welding (SMAW) process with V-bevel and consists of two weld seams, where the heat affected zone is clearly visible. While circumferential welding is a welding of multiple passes, where overheating by the different weld seams makes it difficult to see the thermally affected zone. Figure 5(c) and Figure 5(d) shows an optical microscopy image of base metal and welding microstructure respectively. The base metal shows a homogeneous microstructure with a fine grain size (average grain size of 10 microns). The microstructure of the base metal consisted of predominately ferrite.

3.2. Hardness Measurements

Vickers hardness measurements along the circumferential weld joint of the API X52 steel were carried out as observed in Figure 6. According to NACE MR 0175 [14] a maximum hardness of 22 Rockwell C scale (248 HV) should be permitted in order to avoid SSC problems. The maximum hardness measured was 216 HV (18 HRC) located in the weld bead as is shown in Figure 6.
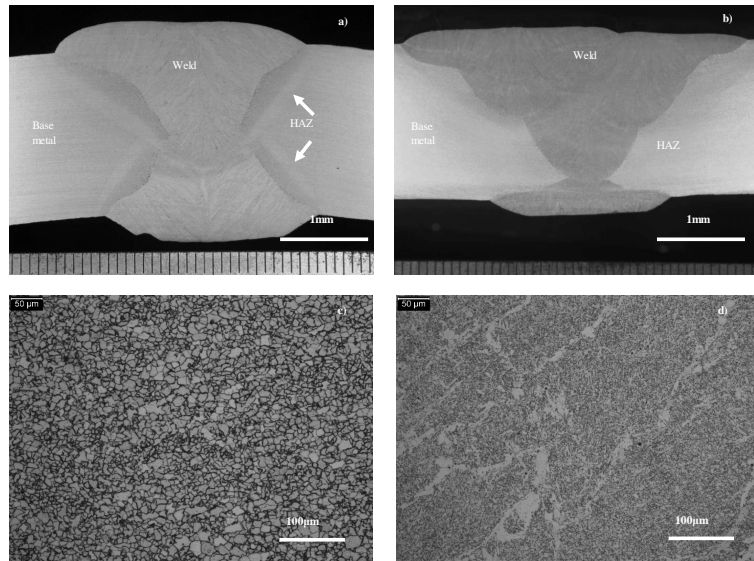
Figure 5. Micrographs obtained by optical microscopy from (a) longitudinal weld, (b) circumferential weld, (c) base metal microstructure, and (d) circumferential weld microstructure.
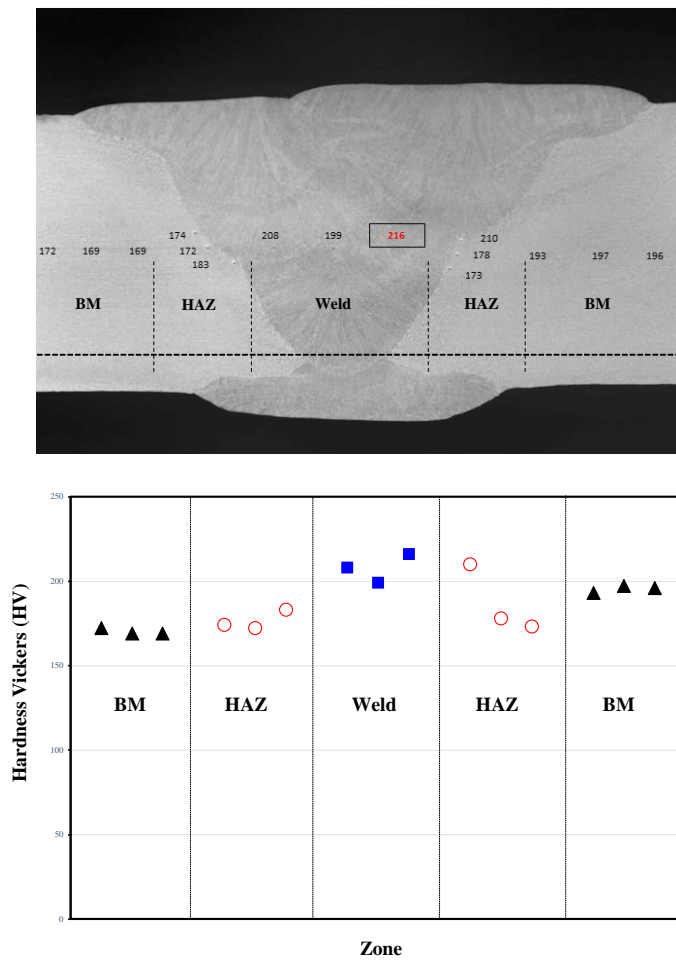

Figure 6. Vickers hardness measurements in the circumferential welding joint of X52 steel.

3.3. Tensile Tests

Tensile tests were performed according to ASTM E21 [15] for each test temperature (25°C, 50°C, 65°C, 80°C and 150°C) in order to characterize the steel before performing the SSC tests. The tensile test results at different temperatures are presented in Table 4. The AYS obtained at different temperatures were used to stress the Four Point Bend Beam specimens. From Table 4 it is observed that YS decreases as temperature of the test increases.

3.4. Hydrogen Induced Cracking Tests (HIC)

HIC tests on samples obtained from API X52 steel with dimensions according to NACE TM 0284 [17] were carried out. The test results, including the average crack sensitivity ratio (CSR), crack length ratio (CLR), and crack thickness ratio (CTR) for each specimen are presented in Table 5.

After specimen's exposure for 96 h, they were removed for sectioning and polish. Cracking was observed only in the specimen removed from the parent material (CS-5) at 90 degrees from the longitudinal weld. The average ratios for this specimen were 8.25% for CLR, 0.097% for CTR and 0.012% for CSR. However, the acceptance criteria of NACE TM 0284 are: CLR less than of the 15%, CTR less than of the 5%, CSR less than 2%, therefore, the values obtained did not exceed the criteria established in NACE TM 0284. All other specimens did not exhibit cracking after metallographic analysis.

Figure 7 shows an optical image of the CS-5 specimen for section B and C after been polished and etched with 2% Nital to reveal the crack path; it was observed that apparently the crack mechanisms was intergranular. These cracks were observed in the metal base.
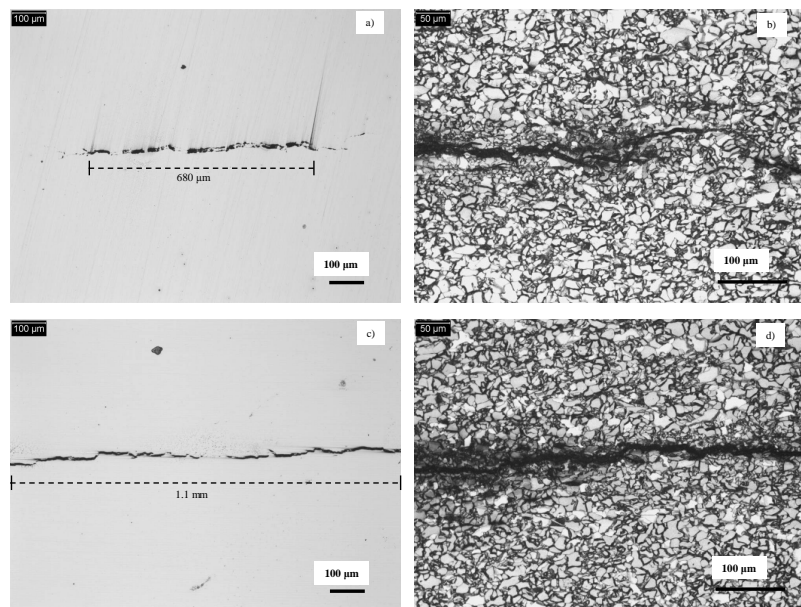

Figure 7. Micrograph of specimen CS-05 (90° from weld): (a) section B at 100× polished only (b) section B at 200× after being attacked with Nital 2%, (c) section C at 100× polished only, and (d) section C at 200× after being attacked with Nital 2%.

Table 4. Tensile test results at different temperatures.

Specimen	Temperature (˚C)	0.2% YS (psi)	Average YS (psi)	80% AYS (psi)
CS-379	25	64,072	64,616	51,693
CS-380		65,160		
CS-381	50	58,624	60,183	48,146
CS-382		61,742		
CS-383	65	63,033	61,075	47,293
CS-384		59,117		
CS-385	80	57,696	57,892	46,313
CS-386		58,087		
CS-387	150	55,926	55,716	44,572
CS-388		55,505		

Table 5. HIC testing results for X52 steel welded joints.

Specimen	Location	Section	CLR (%)	CTR (%)	CSR (%)	Results
CS-01	Circumferential weld	Sec. A	0.000	0.000	0.000	No cracking
		Sec. B	0.000	0.000	0.000	
		Sec. C	0.000	0.000	0.000	
		Average	0.000	0.000	0.000	
CS-02	Circumferential weld	Sec. A	0.000	0.000	0.000	No cracking
		Sec. B	0.000	0.000	0.000	
		Sec. C	0.000	0.000	0.000	
		Average	0.000	0.000	0.000	
CS-03	Longitudinal weld	Sec. A	0.000	0.000	0.000	No cracking
		Sec. B	0.000	0.000	0.000	
		Sec. C	0.000	0.000	0.000	
		Average	0.000	0.000	0.000	
CS-04	Longitudinal weld	Sec. A	0.000	0.000	0.000	No cracking
		Sec. B	0.000	0.000	0.000	
		Sec. C	0.000	0.000	0.000	
		Average	0.000	0.000	0.000	
CS-05	90˚ from weld	Sec. A	0.000	0.000	0.000	Cracking
		Sec. B	12.133	0.144	0.018	
		Sec. C	12.623	0.145	0.018	
		Average	8.252	0.097	0.012	
CS-06	180˚ from weld	Sec. A	0.000	0.000	0.000	No cracking
		Sec. B	0.000	0.000	0.000	
		Sec. C	0.000	0.000	0.000	
		Average	0.000	0.000	0.000	

3.5. Sulfide Stress Cracking Tests

SSC tests were performed according to NACE TM 0177 [18] method B and FPBB specimens from API X52 steel were tested. As described above, the Four Point Bent-Beam (FPBB) specimens were stressed up to 80% of the Actual Yield Strength (AYS) obtained at each test temperature. The results of SSC tests of X52 steel are shown in Table 6. This table includes the material, specimen, test temperature, AYS, stress applied, initial and final pH, and testing results.

Table 6. SSC testing results for X52 steel.

Test No.	Specimen	Temp. (°C)	AYS (psi)	Applied stress (psi)	pH initial	pH final	Surface cracks observed	Sub-Surface cracks observed
	CS-1						No	No
1	CS-2	25	64,616	51,693	3.0	4.5	No	No
	CS-3						No	No
	CS-4						No	No
2	CS-5	25	64,616	51,693	3.0	4.6	No	No
	CS-6						No	No
	CS-19						No	No
3	CS-20	50	60,183	48,146	3.8	4.3	No	No
	CS-21						No	No
	CS-22						No	No
4	CS-23	80	57,892	46,314	3.8	4.8	No	No
	CS-24						No	No
	CS-28						No	No
5	CS-29	50	60,183	48,146	3.5	4.1	No	No
	CS-30						No	No
	CS-25						No	No
6	CS-26	80	57,892	46,314	3.5	4.6	No	No
	CS-27						No	No
	CS-7						No	No
7	CS-8	65	61,075	47,293	3.5	4.4	No	No
	CS-9						No	No
	CS-10						No	No
8	CS-11	150	55,716	44,572	3.5	4.9	No	No
	CS-12						No	No
	CS-13						No	Yes
9	CS-14	150	55,716	44,572	3.5	4.8	No	No
	CS-15						No	No
	CS-34						No	No
10	CS-35	50	60,183	48,146	3.9	4.2	No	No
	CS-36						No	No
	CS-31						No	No
11	CS-32	80	57,892	46,314	3.9	4.3	No	No
	CS-33						No	No

No indications of cracking were observed on any surface specimen's after the exposures to SSC testing, except for specimen CS-13 exposed to the testing conditions No. 9 from Table 3, consisting of solution B saturated with 96 psi of H$_2$S and 53 psi of CO$_2$ at 150˚C. This sample showed subsurface cracks after metallographic examination. Micrographs of the cracks are presented in Figure 8. The specimen CS-13 showed two cracks between the upper and lower weld bead, one on the right and other in the left sides as shown in Figure 8(a). Figure 8(a1) shows a crack between the two weld beads very close to interface between metal base and weld bead. Figure 8(a1) shows a crack that initiated close to fusion zone interface, which propagated through the weld as a consequence of the different microstructures and the properties of each phase. Also, the reheating during the welding process of the second weld bead produced recrystallization and grain growth of the first bead, which makes it more fragile and susceptible to SSC. Figure 8(a2) shows two cracks that seem to have their origin in a weld defect. The remaining specimens did not show any cracks after metallographic examination.

3.6. Corrosion Testing

Corrosion testing was performed on X52 steel coupons according to ASTM G 111 [21]. The coupons were tested in duplicate in each sour environment during 720 hours according to conditions showed in Table 7.

The calculated corrosion rates (CR) for general corrosion and the localized corrosion evaluation for coupons are presented in Table 7 and Table 8 respectively. General corrosion rate was calculated according to Equation (4); meanwhile localized corrosion rate was evaluated according to ASTM G46 [24].
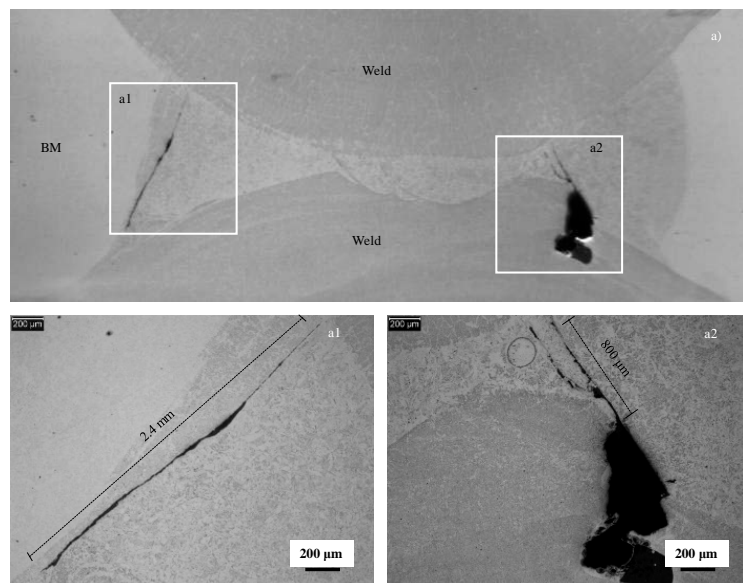

Figure 8. Optical micrographs of X52 weld joint after testing at 96 psi of H$_2$S and 53 psi of CO$_2$ at 150˚C: (a) Microstructure of longitudinal weld joint at 10× showing the presence of two cracks, (a1) higher magnification of the crack a1 at 50×, and (a2) higher magnification of the crack a2 at 50×.

The highest average value for general corrosion rate was 0.27 mm/year (10.6 mpy) corresponding to CS-53 and CS-54 coupons exposed to conditions of high pressure and high temperature (HP/HT); and correspond to the testing conditions No. 9 of Table 7 (96 psi of H_2S and 53 psi of CO_2 at 150˚C). This value can be considered moderate, but should be used as a conservatively value because the tests were performed under static conditions. Some images of this SSC-Four Point Bent-Beam after testing are presented in Figure 9. The lowest average value for general corrosion rate was 0.028 mm/year (1.1 mpy) belong to CS-61 and CS-62 coupons exposed to the testing conditions No. 1 of Table 7 (H_2S at 8 psi; at 25˚C).

Table 7. General corrosion rates for X52 steel coupons.

Test No.	Specimen	Length (in)	Width (in)	Thick (in)	Surface area (in²)	Weight before test (g)	Weight after test-before clean (g)	Weight after test-after clean (g)	CR (mpy)	Average CR (mpy)
1	CS-61	1.999	0.994	0.124	4.716	31.185	31.18	31.133	1	1.1
	CS-62	1.984	0.991	0.124	4.67	30.702	30.695	30.641	1.2	
2	CS-65	1.996	0.995	0.125	4.72	31.3	31.281	31.224	1.5	1.6
	CS-66	1.996	0.993	0.124	4.705	31.316	31.288	31.229	1.7	
3	CS-55	1.993	0.993	0.122	4.687	31.138	31.063	30.934	4.1	4.5
	CS-56	1.995	0.986	0.122	4.662	30.981	30.872	30.742	4.9	
4	CS-59	1.991	0.991	0.123	4.68	30.559	30.574	30.296	5.3	5.3
	CS-60	2.001	0.993	0.124	4.716	31.18	31.217	30.912	5.4	
5	CS-57	1.986	0.985	0.123	4.643	30.791	30.777	30.484	6.3	6.3
	CS-58	1.971	0.988	0.122	4.617	30.519	30.477	30.214	6.3	
6	CS-51	1.997	0.972	0.124	4.618	30.593	30.259	30.241	7.2	6.9
	CS-52	1.991	0.989	0.124	4.677	30.808	30.499	30.483	6.6	
7	CS-63	1.998	0.993	0.124	4.71	31.135	30.938	30.824	6.2	6.2
	CS-64	1.997	0.995	0.123	4.71	31.341	31.158	31.036	6.1	
8	CS-69	1.993	0.99	0.121	4.668	30.877	30.622	30.483	8	8
	CS-70	1.986	0.986	0.121	4.636	30.288	30.052	29.897	8	
9	CS-53	1.986	0.989	0.124	4.666	30.895	30.431	30.411	9.8	10.6
	CS-54	1.992	0.988	0.123	4.669	30.576	30.039	30.017	11.3	
10	CS-71	1.997	0.987	0.121	4.664	30.784	30.763	30.689	1.9	1.8
	CS-72	1.997	0.991	0.122	4.687	31.084	31.071	30.999	1.7	
11	CS-67	1.986	0.982	0.123	4.631	30.67	30.623	30.555	2.4	2.5
	CS-72	1.997	0.991	0.122	4.687	31.084	31.071	30.999	1.7	

Table 8. Localized corrosion rates for X52 steel coupons.

Test No.	Specimen	Max. Pit Depth (mils)	Max. Pit Depth (mm)	Corrosion rate (mpy)	Observations
1	CS-61	0.4	0.01	4.795	General Corr. Attack on surface
	CS-62	0.5	0.013	6.234	
2	CS-65	0.6	0.015	7.193	General Corr. Attack on surface
	CS-66	1.3	0.033	15.825	
3	CS-55	2	0.051	24.456	Loc. Corr. Attack on selective areas
	CS-56	1.8	0.046	22.059	
4	CS-59	2.8	0.071	34.047	Loc. Corr. Attack on selective areas
	CS-60	1.5	0.038	18.222	
5	CS-57	2.8	0.071	34.047	General Corr. Attack on surface
	CS-58	3.9	0.099	47.474	
6	CS-51	6.5	0.165	79.124	Loc. Corr. Attack on selective areas
	CS-52	2.8	0.071	34.047	
7	CS-63	3.5	0.089	42.679	Loc. Corr. Attack on selective areas
	CS-64	3	0.076	36.445	
8	CS-69	11	0.279	133.791	Severe pitting attack
	CS-70	12.6	0.32	153.452	
9	CS-53	13.4	0.34	163.043	Severe pitting attack
	CS-54	13.7	0.348	166.879	
10	CS-71	1.4	0.036	17.263	Loc. Corr. Attack on selective areas
	CS-72	1.7	0.043	20.620	
11	CS-67	0.8	0.02	9.591	Loc. Corr. Attack on selective areas
	CS-72	3.0	0.076	36.445	
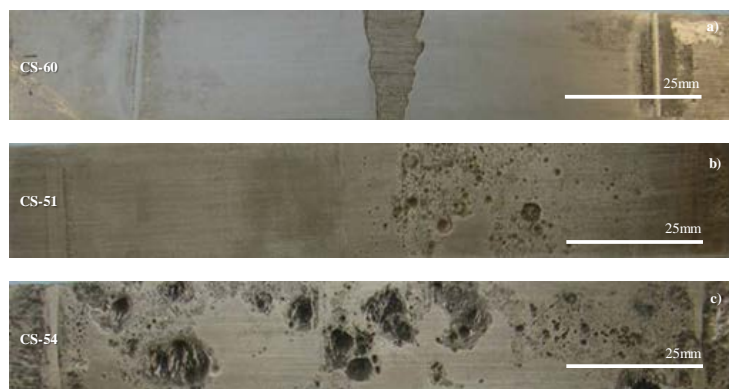
Figure 9. Images of X52 steel SSC-FPBB after being exposed to environment: (a) No. 4 (CS-60), (b) No. 6 (CS-51), and (c) No. 9 (CS-54).

The localized corrosion rate was evaluated according to ASTM G46 [23]. For this purpose, all the coupons were analyzed through optical microscopy; then measurements of pitting depth using a micrometer were carried out. Table 8

shows the corrosion rate for each specimen.

The surface of the specimens through optical microscopy was analyzed in order to determine localized corrosion (pitting). Figure 10 shows images obtained by optical microscopy of the pitting corrosion on the surface of CS-60, CS-51 and CS-54 steel coupons. The corrosion-pitting rate was calculated for these specimens exposed to environment No. 4, No. 6 and No. 9 was 18.22, 79.12 and 166.87 mpy, respectively. The observed severe pitting in these coupons can be attributed to high H_2S and CO_2 content at high temperature that make possible the formation of a non-homogeneous layer of iron sulfides products and iron carbonates/bicarbonates combinations.

The presence of H_2S at low partial pressures can induce the formation of sulfides layers reducing the corrosion rate; however, at temperatures above 50˚C, the films can become unstable with the exposure time giving origin to pitting.
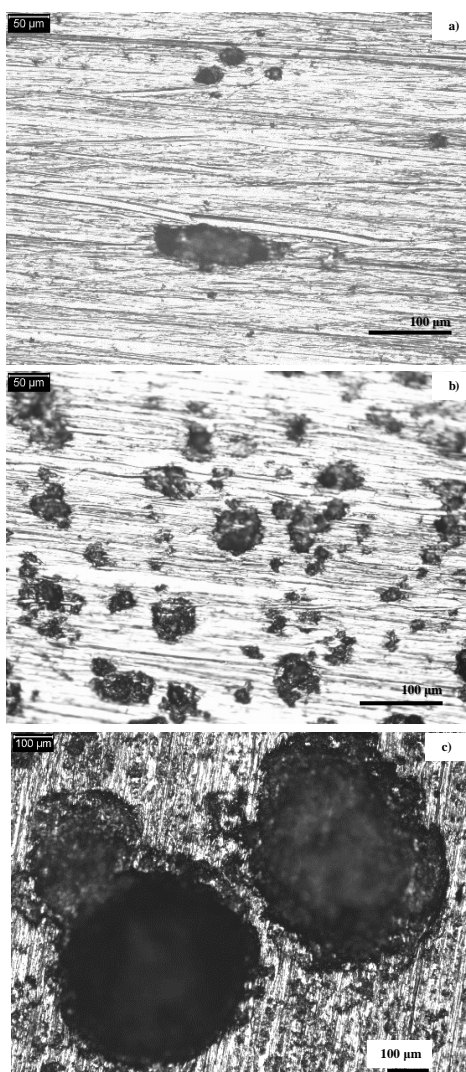

Figure 10. Images of pitting morphology generated on the surface of X52 steel after being exposed to environment: (a) No. 4 (CS-60), (b) No. 6 (CS-51), and (c) No. 9 (CS-54).

As expected, a black scale was observed in all specimen's surfaces after testing due to the presence of sulfides. Localized corrosion (pitting) in all specimens of X52 steel exposed to sour environments was observed. The specimen, CS-54 exposed to environment No. 9 (96 psi H_2S and 53 psi CO_2 at 150˚C), presented the deepest pit measured. The pit depth was 0.348 mm (13.7 mils) that corresponds to a corrosion rate of 4.2 mm/year (167 mpy). It was also observed that HP/HT environments not only generate the deepest pitting, but also these pits grow in extension as shown in Figure 10(c).

Comparing the general corrosion rate against localized corrosion rate at high temperature (150˚C) and high concentrations of H_2S and CO_2 (96 psi H_2S and 53 psi CO_2; test 9 from Table 3), the calculated average corrosion rate was 10.6 and 164 mpy, respectively. As expected, the localized corrosion (pitting) rate is higher than general corrosion rate.

3.7. Influencing H_2S/CO_2 Corrosion

The damage caused by H_2S occurred in two types, localized corrosion or general corrosion, which depend upon the type and nature of formed corrosion product. H_2S corrosion has been claimed to be strongly dependent on chloride ion concentration with severe damage rate. However, the presence of other corrosive agents and/or fluid chemistry on the corrosion rate degradation is unknown [24] [25]. The corrosion reaction often leads to the formation of iron sulfide (FeS) scales, which under certain conditions are highly protective. However, when they fracture (*i.e.* under turbulent flow conditions) can lead to severe localized corrosion in a similar manner for $FeCO_3$ cracking with CO_2 corrosion [26]. The kinetics and nature of FeS film formation, stabilizes and contribute to reduce corrosion rate, therefore they are the key for corrosion protection. Similarly, to CO_2 corrosion, the corrosion rate of H_2S is affected by: fluid chemistry, organic acids and fluids flow velocity in addition to the presence of elemental Sulphur. It has been identified that the ability of H_2S to affect acidity is indicated by its ionization as follows:

$$H_2S \leftrightarrow H^+ + HS^- \tag{5}$$

From Equation (5), it can be observed that as the term H^+ is removed through the cathodic reaction of hydrogen reduction, more is formed, leading to the appearance of hydrogen gas on steels exposed to oxygen and free water containing H_2S as follows:

$$2H^+ + 2e \rightarrow 2H\left(\text{atomic hydrogen}\right) \rightarrow H_2\left(\text{molecular hydrogen}\right) \tag{6}$$
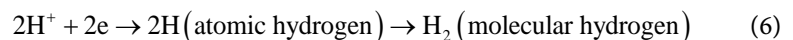
Then, the anion (HS^-) dissociates further to S^{2-} and H^+. Therefore, the S^{2-} ion reacts with iron to form the black FeS corrosion product commonly found in service. H_2 may not be present in the bulk solution, but it can be formed locally within the corrosion layer as a cathodic corrosion product, diffusing from its electrochemical production at the metal surface to its final dispersion in the bulk at the outer surface (contact surface).

As a general, in CO_2 containing environments the presence of H_2S can:

- Increase the corrosion risk by either:
- ✧ Facilitating localized corrosion, at a higher rate than the general metal loss or localized rate expected from CO_2 corrosion, or:
- ✧ Preferentially forming an FeS corrosion product, which is less protective than an iron carbonate corrosion product.
- Decrease the corrosion risk by promoting the formation of films of FeS through either:
- ✧ Replacing a less protective iron carbonate film, or:
- ✧ Forming a combined iron sulfide and iron carbonate protective layers.

It can also be observed that in the presence of both acid gases, the dominant acid gas governs the corrosion process.

The presence of H_2S in CO_2 contents, in oil and gas production environments, has been reviewed by Pots *et al.* [24]. Who introduced a notion of CO_2/H_2S ratio and considered three different corrosion domains, based on the dominance corrosion mechanism affected by the dominating acid gas, as follows:

$$CO_2/H_2S < 20 \tag{7}$$

- ✧ Corrosion dominated by H_2S (FeS as the main corrosion product)

$$20 < CO_2/H_2S < 500 \tag{8}$$

- ✧ Mixed CO_2/H_2S corrosion dominance (a mixture of FeS and $FeCO_3$ as the main corrosion products)

$$CO_2/H_2S > 500 \tag{9}$$

- ✧ CO_2 corrosion dominates ($FeCO_3$ as the main corrosion product).

As expected, according to Equations (7) and (8), the CO_2/H_2S ratio, results obtained from Table 3, the corrosion damage pattern is the formation of a mixture of FeS and $FeCO_3$ protective film. The possible formation of a non-homogeneous layer of combination of iron sulfide products and iron carbonates/bicarbonates occurred because initially, the pH value can promote a less reactive metal-liquid interface, and subsequently during exposure to temperature of 150°C the film of the corrosion products is weakened, inducing the generation of deep corrosion pitting along the surface exposed to HP/HT conditions.

In the oil and gas industry, it has been established that for pipelines fabricated with carbon steels, their limitation is related to H_2S and CO_2 environments, which is 7 to 10 psia of partial pressure of CO_2, as indicated in Figure 11. Therefore, in carbon steel, after 7 or 10 psia of partial pressure of CO_2, the steel shows cracks. However, under the conditions of the tests carried out, the oil and gas industry use carbon steels pipelines in partial pressure higher than 10 psia of CO_2 (Figure 11), considering corrosion rate and the pitting speed values, during a determined life service, the pipelines are replaced by new carbon steel pipelines.

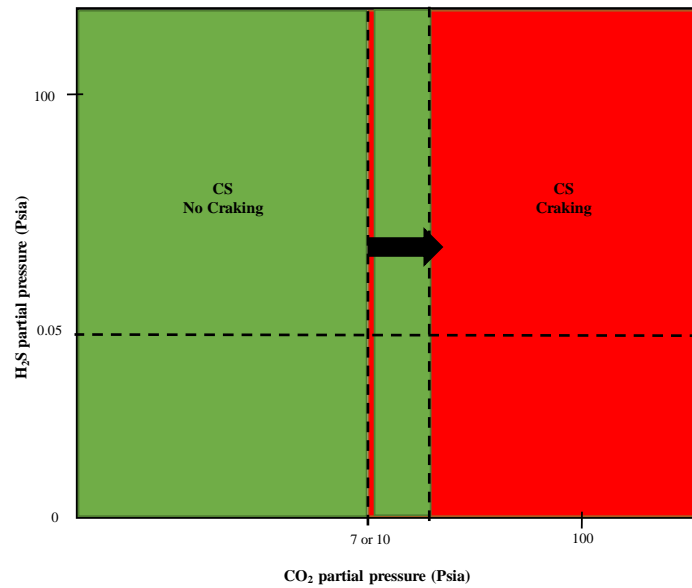The operational parameters affecting CO_2-H_2S corrosion rate:

Figure 11. Cracking limits for carbon steel pipelines as function partial pressure of H_2S and CO_2.

- CO_2/H_2S ratio.
- Temperature.
- Fluid Chemistry (water chemistry, pH, organic acids, water cut, oil wettability, phase ratios, etc.).
- The hydrocarbon phase.
- Flow characteristics and fluid velocity.
- Steel surface.
- Corrosion products, such as: scales, wax and asphaltenes.
- Steel chemistry.

4. Conclusions

According to the results obtained from the qualification tests of X52 steel to be used in fields at high pressure and high temperature we can draw the following conclusions:

- The oil and gas industry could use carbon steels pipelines in partial pressure higher than 10 psia of CO_2. X52 steel is not susceptible to HIC or SSC phenomenon at the studied conditions; however, the values of the corrosion rate are considered moderate, but under conditions of hydrodynamic flow regime they can be greatly increased.
- In the combined environment of CO_2 and H_2S, there is a competitive interaction between $FeCO_3$ and FeS corrosion products leading to cracking and/or rupture of protecion layers, resulting in progressive localized corrosion.
- Vickers hardness measurements were made on the welded joints of X52 steel obtaining the maximum hardness in the weld beads (216 HV) which meets the requirements established in NACE MR 0175/ISO 15156 (maximum 248 HV).

- Tensile tests were performed according to ASTM E21 for each test temperature in order to characterize the steel before performing the SSC. The average yielding stress (AYS) used in SSC tests by Four Point Bend Beam technique decreases as temperature of the test increases.

- The results of HIC tests, performed according to NACE TM 284, showed that welding joints did not exhibit cracks, except for specimen CS-5 obtained from the base metal at 90 degrees from the longitudinal weld. However, the obtained values did not exceed the criteria established in NACE TM 0284.

- Results of SSC did not show indications of cracking after the exposure to sour solutions, except specimen CS-13, which was exposed to solution B saturated with 96 psi of H_2S and 53 psi of CO_2 at 150˚C. This sample showed subsurface cracks after metallographic examination, located between the upper and lower weld bead, and some of them seem to have their origin from a welding defect.

- The highest average value for general corrosion rate was 0.27 mm/year (10.6 mpy) corresponding to CS-53 and CS-54 coupons exposed to the testing conditions of 96 psi H_2S and 53 psi CO_2 at 150˚C. These values can be considered conservatively because the tests were performed under static conditions.

- Localized corrosion (pitting) in all specimens of X52 steel exposed to the sour environments was observed. Specimen CS-54 exposed to environment No. 9 (96 psi H_2S and 53 psi CO_2 at 150˚C) presented the deepest pit measured 0.348 mm (13.7 mils) that correspond to a corrosion rate of 4.2 mm/year (167 mpy).

- Comparing the general corrosion rate with localized corrosion rate at high temperature (150˚C) and high concentrations of H_2S and CO_2 (96 psi H_2S and 53 psi CO_2), the calculated average corrosion rate was 10.6 and 164 mpy, respectively. As expected, the localized corrosion (pitting) rate is higher than general corrosion rate.

Acknowledgements

Conflicts of Interest

The author declares no conflicts of interest regarding the publication of this paper.

References

[1] de Assis, K.S., Schuabb, C.G.C., Lage, M.A., Gonçalves, M.P.P., Dias, D.P. and Mattos, O.R. (2019) Slow Strain Rate Tests Coupled with Hydrogen Permeation: New Possibilities to Assess the Role of Hydrogen in Stress Corrosion Cracking Tests Part

I: Methodology and Commissioning Results. *Corrosion Science*, **152**, 45-53. https://doi.org/10.1016/j.corsci.2019.02.028

[2] Zvirko, O., Gabetta, G., Tsyrulnyk, O. and Kret, N. (2019) Assessment of In-Service Degradation of Gas Pipeline Steel Taking into Account Susceptibility to Stress Corrosion Cracking. *Procedia Structural Integrity*, **16**, 121-125. https://doi.org/10.1016/j.prostr.2019.07.030

[3] Nykyforchyn, H., Krechkovska, H., Student, O. and Zvirko, O. (2019) Feature of Stress Corrosion Cracking of Degraded Gas Pipeline Steels. *Procedia Structural Integrity*, **16**, 153-160. https://doi.org/10.1016/j.prostr.2019.07.035

[4] Roccisano, A., Nafisi, S. and Ghomashchi, R. (2020) Stress Corrosion Cracking Observed in Ex-Service Gas Pipelines: A Comprehensive Study. *Metallurgical and Materials Transactions A*, **51**, 167-188. https://doi.org/10.1007/s11661-019-05496-3

[5] Wang, Q., Sun, Y., Shi, G., Meng, K., Wang, Q. and Zhang, F. (2020) Effect of Niobium on Sulfide Stress Cracking Behavior of Tempered Martensitic Steel. *Corrosion Science*, **165**, Article ID: 108387. https://doi.org/10.1016/j.corsci.2019.108387

[6] Rahimi, S. and Marrow, T.J. (2020) A New Method for Predicting Susceptibility of Austenitic Stainless Steels to Intergranular Stress Corrosion Cracking. *Materials & Design*, **187**, Article ID: 108368. https://doi.org/10.1016/j.matdes.2019.108368

[7] Gong, K., Wu, M. and Liu, G. (2020) Stress Corrosion Cracking Behavior of Rusted X100 Steel under the Combined Action of Cl^- and HSO_3^- in a Wet-Dry Cycle Environment. *Corrosion Science*, **165**, Article ID: 108382. https://doi.org/10.1016/j.corsci.2019.108382

[8] Saleem, B., Ahmed, F., Rafiq, M.A., Ajmal, M. and Ali, L. (2014) Stress Corrosion Failure of an X52 Grade Gas Pipeline. *Engineering Failure Analysis*, **46**, 157-165. https://doi.org/10.1016/j.engfailanal.2014.08.011

[9] Fang, B.Y., Eadie, R.L., Chen, W.X. and Elboujdaini, M. (2010) Pit to Crack Transition in X-52 Pipeline Steel in Near Neutral pH Environment Part 1—Formation of Blunt Cracks from Pits under Cyclic Loading. *Corrosion Engineering, Science and Technology*, **45**, 302-312. https://doi.org/10.1179/147842208X386304

[10] Pessu, F., Barker, R. and Neville, A. (2017) Pitting and Uniform Corrosion of X65 Carbon Steel in Sour Corrosion Environments: The Influence of CO_2, H_2S, and Temperature. *CORROSION*, **73**, 1168-1183. https://doi.org/10.5006/2454

[11] Shoesmith, D.W., Taylor, P., Bailey, M.G. and Ikeda, B. (1978) Electrochemical Behaviour of Iron in Alkaline Sulphide Solutions. *Electrochimica Acta*, **23**, 903-916. https://doi.org/10.1016/0013-4686(78)87014-5

[12] Henriques, C.C.D., Joia, C.-J.B., Guedes, F. and Baptista, I.P. (2012) Material Selection for Brazilian Presalt Fields. 2012 *Offshore Technology Conference*, Houston, 30 April-3 May 2012, 1-11. https://doi.org/10.4043/23320-MS

[13] Henriques, C.C.D., Joia, C.-J.B., Guedes, F. and Baptista, I.P. (2012) Materials Design Strategy: Effects of H_2S/CO_2 Corrosion on Materials Selection. 2012 *Offshore Technology Conference*, San Diego, CA, USA, 12-16 March 2012, 1-18. https://www.onepetro.org/conference-paper/NACE-06121

[14] National Association of Corrosion Engineers (2015) Petroleum and Natural Gas Industries—Materials for Use in H_2S-Containing Environments in Oil and Gas Production. ANSI/NACE MR0175/ISO 15156, Houston, USA.

[15] American Society for Testing and Materials (2017) Standard Test Methods for Elevated Temperature Tension Tests of Metallic Materials. ASTM E21, West Conshohocken, PA, USA. https://www.astm.org/DATABASE.CART/HISTORICAL/E21-17.htm

[16] American Society for Testing and Materials (2016) Standard Test Methods for Tension Testing of Metallic Materials. ASTM E8, West Conshohocken, PA, USA.
https://www.astm.org/Standards/E8.htm

[17] American National Standards Institute and National Association of Corrosion Engineers (2011) Standard Test Evaluation of Pipeline and Pressure Vessel Steels for Resistance to Hydrogen-Induced Cracking. ANSI/NACE TM0284, 20.
https://www.mendeley.com/catalogue/standard-test-method-evaluation-pipeline-pressure-vessel-steels-resistance-hydrogeninduced-cracking-1/

[18] National Association of Corrosion Engineers (2016) TM0177-2016-SG, Laboratory Testing of Metals for Resistance to Sulfide Stress Cracking and Stress Corrosion Cracking in H_2S Environment. National Association of Corrosion Engineers, Houston.

[19] European Federation of Corrosion (2013) Guidelines on Material Requirements for Carbon and Low Alloy Steels for H_2S-Containing Environments in Oil and Gas Production. Publication No. 16.
https://es.scribd.com/doc/142021712/EFC-16-Guidelines-on-Materials-Requirements-for-Carbon-and-Low-Alloy-Steels-for-H_2S-Containing-Environments-in-Oil-and-Gas-Production-pdf

[20] American Society for Testing and Materials (2014) Standard Test Method for Hydrophobic Surface Films by the Atomizer Test. ASTM F21-20.
https://www.astm.org/search/fullsite-search.html?query=F21&

[21] American Society for Testing and Materials (2018) Standard Guide for Corrosion Tests in High Temperature or High Pressure Environment, or Both. ASTM G111-97.
https://www.astm.org/search/fullsite-search.html?query=G111&

[22] American Society for Testing and Materials (2017) Standard Practice for Preparing, Cleaning, and Evaluating Corrosion Test Specimens. ASTM G1-03.
https://www.astm.org/search/fullsite-search.html?query=G1&

[23] American Society for Testing and Materials (2018) Standard Guide for Examination and Evaluation of Pitting Corrosion. ASTM G46-94.
https://www.astm.org/Standards/G46

[24] Pots, B.F.M., Kapusta, S.D., John, R.C., Simon Thomas, M.J.J., Rippon, I.J., Whitham, T.S. and Girgis, M. (2002) Improvements on de Waard-Milliams Corrosion Prediction and Applications to Corrosion Management. National Association of Corrosion Engineers, Denver, USA

[25] Bich, K. and Goerz N.N. (1996) Caroline Pipeline Failure: Findings on Corrosion Mechanisms in Wet Sour Gas Systems Containing Significant CO_2. *National Association of Corrosion Engineers Annual Corrosion Conference and Exposition: Water and Waste Water Industries*, Denver, 24-29 March 1996, 1-14.

[26] Kermani, M.B. and Morshed, A. (2003) Carbon Dioxide Corrosion in Oil and Gas Production—A Compendium. *CORROSION*, **59**, 659-683.
https://doi.org/10.5006/1.3277596